POLITECNICO DI TORINO
Repository ISTITUZIONALE

Co-design for social impact and inclusion. 25 competencies by the ATELIER Project

Original
Co-design for social impact and inclusion. 25 competencies by the ATELIER Project / Campagnaro, C., Ceraolo, S., Curtabbi, G., Brileanu, P.I., Ciampolini, T., Dima, G., Fantasia, A., Koimisoglou, M., Lalli, I., Oliveira, J.P., Oliveira, M., Pitkäkangas, L., Tornariti, E., Tsanakas, T., Zarzyska, A.. - ELETTRONICO. - (2026), pp. 1-435.

Availability:
This version is available at: 11583/3013701 since: 2026-07-29T11:48:15Z

Publisher:
Politecnico di Torino

Published
DOI:

Terms of use:

This article is made available under terms and conditions as specified in the corresponding bibliographic description in the repository

Publisher copyright

(Article begins on next page)

11 September 2026

Engineering Fracture Mechanics 292 (2023) 109597

Contents lists available at ScienceDirect

Engineering Fracture Mechanics

journal homepage: www.elsevier.com/locate/engfracmech

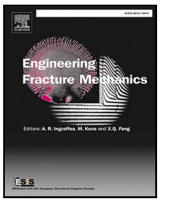

Analytical computation of stress intensity factor for active material particles of lithium ion batteries

Francesca Pistorio *, Davide Clerici, Aurelio Somà

Department of Mechanical and Aerospace Engineering, Politecnico di Torino, Corso Duca degli Abruzzi, 24, 10129, Torino, Piemonte, Italy

ARTICLE INFO

Keywords:
Lithium ion batteries
Fracture mechanics
Diffusion induced stress (DIS)
Stress intensity factor (SIF)
Finite element method (FEM)

ABSTRACT

The stress intensity factor is a widely used parameter in linear elastic fracture mechanics to assess the stress field near the crack tip, and it is usually defined as the product between the remote stress, the square root of the crack length, and a geometric factor depending on the geometry of the test specimen, the size and location of the crack. However, this well-established expression cannot be used in case of non-constant stress distribution on crack surfaces, typically resulting from diffusive field. This work presents an analytical procedure to compute the stress intensity factor due to any kind of stress distribution that can be expressed as a polynomial. Firstly, the non-constant stress distribution is expressed as a polynomial. Then, the stress intensity factor is computed according to the principle of superposition of effects, as the sum of the stress components of each single polynomial grade and the corresponding geometric factors. The geometric factors for sphere with central and superficial cracks are determined using a finite element model, and closed-form expressions for these geometric factors are provided as functions of a normalized geometric parameter. These functions can be used in case of any stress loading and spherical geometry. The analytical procedure is specifically applied to assess the stress intensity factor caused by stress resulting from lithium diffusion in active material particles of lithium ions batteries electrodes. The results are compared with those obtained using a multiphysics finite element fracture model, showing good agreement and demonstrating the accuracy of the proposed analytical procedure. Then, the procedure presented in this work enables avoiding expensive multiphysics simulations and can be used to develop fast, accurate, and computationally efficient lithium ion batteries degradation models for the online estimation of the capacity decay with charge/discharge cycles.

1. Introduction

The stress intensity factor (SIF) is the most used parameter in linear elastic fracture mechanics (LEFM) theory to assess the singularity of the stress field at the crack tip [1–3].

The accurate estimation of SIF is essential to predict the fracture behavior of components under different loading conditions. For instance, the criterion of maximum circumferential stress used to determine the crack propagation path depends on SIF values [4], as well as the Paris' law predicting the fatigue life of components due to cyclic loads is a function of SIF range [5,6]. For this reason, the development of several techniques to determine SIF has been of particular interest in LEFM.

The magnitude of SIF depends on the geometry of the specimen, the size and location of the crack, and the magnitude of the applied stress [3].

* Corresponding author.
E-mail address: francesca.pistorio@polito.it (F. Pistorio).

https://doi.org/10.1016/j.engfracmech.2023.109597
Received 1 August 2023; Received in revised form 28 August 2023; Accepted 4 September 2023
Available online 9 September 2023
0013-7944/© 2023 The Author(s). Published by Elsevier Ltd. This is an open access article under the CC BY license (http://creativecommons.org/licenses/by/4.0/).

Nomenclature

Symbols

σ_i	ith coefficient of polynomial stress distribution (MPa)
θ	Polar coordinate in crack reference frame (–)
a	Crack length (m)
c	Concentration (mol/m^3)
c_R	Reference concentration (mol/m^3)
D	Diffusion coefficient (m^2/s)
D_{eqv}	Equivalent diffusion coefficient for coupled model (m^2/s)
E	Young modulus (MPa)
F	Faraday constant (As/mol)
f_{ij}	Dimensionless shape function
I	Current density (A/m^2)
K	Stress intensity factor (MPa m$^{0.5}$)
k_m	Mechanical coupling parameter (m^3/mol)
n_i	Normal versor (–)
R	Active material particle radius (m)
r	Radial coordinate (–)
r_c	Polar coordinate in crack reference frame (–)
R_g	Gas constant (J/mol K)
T	Temperature (K)
t	Time (s)
t_i	Traction vector (MPa)
T_R	Reference temperature (K)
u	Particle level displacement (m)
W	Strain energy density (J/m^3)
x_1	Coordinate direction along crack extension
x_2	Coordinate direction perpendicular to crack extension
Y	Geometric factor

Acronyms

CZM	Cohesive zone model
DF	Diffusive field
DIS	Diffusion induced stress
FEM	Finite element model
LEFM	Linear elastic fracture mechanics
LIB	Lithium ions battery
PFM	Phase field model
SIF	Stress intensity factor
SOC	State of charge (%)
WFM	Weight function method

Greek Symbols

α	Expansion coefficient (1/K)
ϵ^c	Diffusion strain (–)
ϵ^T	Thermal strain (–)
ϵ_c	Hoop strain (–)
ϵ_r	Radial strain (–)
Γ	Path

Several analytical solutions of SIF considering different geometries and loading conditions have been developed over the years and are collected in well-known handbooks [7–10]. The main drawback of analytical solutions is that they can be applied to a limited number of standard cases, despite the ease of computation. On the other hand, numerical computation based on the finite element

Λ	Area enclosed in the path Γ
ν	Poisson ratio (−)
Ω	Partial molar volume (m^3/mol)
σ_c	Hoop stress (MPa)
σ_h	Hydrostatic stress (MPa)
σ_r	Radial stress (MPa)

Recursive superscripts

max	Maximum

method (FEM) or the weight function method (WFM) is often employed in the case of complex geometry or loading conditions, such as non-uniform stress distribution on crack surfaces.

The diffusion process in solid material causes the migration of energy or chemical species driven by temperature gradient for thermal problem or the concentration gradient for mass transfer problem. The inhomogeneous distribution of the diffusion species results in differential strain, then strain mismatch arises in the material, leading to the so-called diffusion induced stress (DIS) [11,12], which can trigger fracture ultimately.

Several works have addressed a wide range of fracture problems due to stress caused by temperature gradient [13], including thermal shocks problems [14–20].

Regarding fracture caused by chemical diffusion, an important application is on active material particles in electrodes of lithium ion batteries (LIBs). Indeed, fracture is one of the main causes of aging and degradation in LIBs, then a deep understanding of the fracture mechanics in LIBs is essential, given the rapid spread of this technology [21,22].

Fracture in electrodes active material have been studied over the years using both experimental [23] and numerical modeling approaches [24]. Despite the different mechanisms and factors triggering and enhancing fracture, it is observed that the geometry and microstructure of electrodes as well as the current rate affect fracture [25]. In particular, since the current rate is considered a LIB requirement, the appropriate electrode design giving the best trade-off between electrochemical performances, manufacturing cost, and mechanical damage should be chosen.

During LIB operations, lithium ions move between electrodes and get into their microstructure with insertion and extraction processes. Lithium ions distribution in active material particles is inhomogeneous because of diffusion: the concentration is greater at the particle surface with respect to the core during insertion, and vice-versa during extraction. Furthermore, lithium ions insertion and extraction cause the volume change of the particle, which is proportional to lithium concentration: the greater the lithium ions concentration, the greater the volume change of the particle. Then, strain mismatch arises in the particle as areas with higher lithium concentration swell more than areas with lower lithium concentration. This differential strain causes DIS, resulting in crack propagation in electrode microstructure [26–32].

Finally, fracture of electrode microstructure causes impedance rise and capacity fade ultimately, because it isolates some portions of active material, hindering the passage of lithium ions, and triggers undesired side reactions, consuming lithium ions [23].

DIS distribution on crack surfaces of active material particles of LIBs is non-constant. Then, SIF is usually computed with FEM using the path-independent J-integral formulation developed for diffusive-mechanical phenomena [33–37], as analytical solutions are not available. However, the computation is often highly demanding, especially because the solution of a multi-physics problem is required.

Alternatively, SIF is computed according to the WFM [38–42], using a simpler load case to obtain the reference solution. However, the reference solution is usually got from an approximated geometry (plate or disk), as it does not exist for spherical geometry. Clearly, this approximation may affect the accuracy of SIF computation.

Alternative methods to study fracture in LIBs, such as Cohesive Zone Model (CZM) [40,43–50] and Phase Field Model (PFM) [51–61] may be computationally expensive as well.

This work provides a fast, accurate, and computationally efficient analytical procedure to compute SIF in case of non-constant stress distribution on the crack surfaces, typically resulting from a diffusive field, such as the concentration gradient in active material particles of LIBs electrodes. The non-constant stress distribution is expressed as a polynomial and SIF is computed according to the principle of superposition of effects, as the sum of the stress component of each single polynomial grade and the corresponding geometric factor. A spherical geometry with central and superficial cracks is considered. A FEM model is built to compute a general expressions of the geometric factors as a function of the normalized crack length (crack length divided by the radius of the sphere). Finally, the validity of the proposed analytical procedure to compute SIF in active material particles of LIBs electrodes is demonstrated by comparing the analytical results with the multiphysics FEM fracture model results.

The article is organized as follows. The electrochemical–mechanical model to solve lithium concentration, stress, and strain distribution in active material particles of LIBs electrodes is provided in Section 2.1. The basis of LEFM theory and the analytical method for SIF computation based on the principle of superposition of effects are provided in Section 2.2. The implementation of the analytical procedure to compute SIF in case of non-uniform stress distribution on crack surfaces is described in Section 2.3. Closed-form expressions of the geometric factors for sphere with central and superficial cracks and the results of the analytical computation of SIF for graphite particles are shown in Section 3.

Table 1
DIS model equations [12].

Diffusive equations		
Mass conservation	$\frac{\partial c}{\partial t} = \frac{D}{r^2}\frac{\partial}{\partial r}\left(r^2\frac{\partial c}{\partial r}\right)$	(1)
Boundary conditions	$\begin{cases} \left.\frac{\partial c}{\partial r}\right\|_{r=0} = 0 & \text{for } t \geq 0 \\ \left.\frac{\partial c}{\partial r}\right\|_{r=R} = \frac{Rc_{max}C_{rate}}{3\cdot 3600} & \text{for } t \geq 0 \end{cases}$	(2)
Mechanical equations		
Constitutive	$\varepsilon_r = \frac{1}{E}\left[\sigma_r - 2\nu\sigma_c\right] + \frac{\Omega}{3}(c - c_R) \quad \varepsilon_c = \frac{1}{E}\left[(1-\nu)\sigma_c - \nu\sigma_r\right] + \frac{\Omega}{3}(c - c_R)$	(3)
Congruence	$\varepsilon_r = \frac{du}{dr} \quad \varepsilon_c = \frac{u}{r}$	(4)
Equilibrium	$\frac{\partial \sigma_r}{\partial r} + \frac{2}{r}\left(\sigma_r - \sigma_c\right) = 0$	(5)
Boundary conditions	$u\Big\|_{r=0} = 0 \quad \sigma_r\Big\|_{r=R} = 0$	(6)
Solutions		
Concentration	$c(r,t) = c_0 + \frac{IR}{FD}\left[3\tau + \frac{1}{2}\left(\frac{r}{R}\right)^2 - \frac{3}{10} - 2\frac{R}{r}\sum_{n=1}^{\infty}\left(\frac{sin(\lambda_n r/R)}{\lambda_n^2 sin(\lambda_n)}e^{-\lambda_n^2\tau}\right)\right]$	(7)
Displacement	$u(r) = \frac{\Omega}{3(1-\nu)}\left[(1+\nu)\frac{1}{r^2}\int_0^r (c - c_R)r^2\,dr + 2(1-2\nu)\frac{r}{R^3}\int_0^R (c - c_R)r^2\,dr\right]$	(8)
Radial stress	$\sigma_r(r) = \frac{2\Omega}{3}\frac{E}{1-\nu}\left[\frac{1}{R^3}\int_0^R (c - c_R)r^2\,dr - \frac{1}{r^3}\int_0^r (c - c_R)r^2\,dr\right]$	(9)
Hoop stress	$\sigma_c(r) = \frac{\Omega}{3}\frac{E}{1-\nu}\left[\frac{2}{R^3}\int_0^R (c - c_R)r^2\,dr + \frac{1}{r^3}\int_0^r (c - c_R)r^2\,dr - (c - c_R)\right]$	(10)

2. Material and methods

2.1. Electrochemical–mechanical model

In this work, the electrochemical–mechanical model aims to compute the concentration distribution of lithium ions in active material particles of electrodes due to the lithium flux at the particle boundary, depending on the current delivered by the battery. Then, the resulting stress and strain are computed according to the concentration distribution. The main equations of the model along with the boundary conditions are given in Table 1.

The problem is multiphysics and consists of: (a) transport equation, namely the mass transfer equation (Eq. (1)), which is analogous to the heat transfer equation and describes how lithium diffusion (analogous to heat transfer) causes the concentration c (analogous to temperature T) to change with time; (b) stress–strain equations, namely constitutive (Eq. (3)), congruence (Eq. (4)) and equilibrium (Eq. (5)) equations.

The active material particle is modeled as a sphere, and the material is assumed isotropic, homogeneous, and linear elastic [25]. Then, the problem is one-dimensional thanks to the hypothesis of axisymmetry, and the equations are written as a function of just the radial coordinate (r).

The stress–strain equations governing the mechanical field caused by lithium diffusion are analogous to stress–strain equations including thermal effects. Indeed, lithium diffusion causes chemical strain (Eq. (11)a) which is analogous to thermal strain caused by temperature variation (Eq. (11)b).

$$\varepsilon^{DF} = \begin{cases} \frac{\Omega}{3}\left(c - c_R\right) & \text{Chemical strain } (DF = c) \quad \text{(a)} \\ \alpha(T - T_R) & \text{Thermal strain } (DF = T) \quad \text{(b)} \end{cases} \tag{11}$$

Where ε^{DF} is the strain due to diffusive field (chemical or thermal field), Ω is the partial molar volume of active material, α is the coefficient of thermal expansion and $(c - c_R)$, and $(T - T_R)$ are the concentration and temperature variation net of the reference state (c_R and T_R), respectively. Then, the total strain in the constitutive equation has two contributions, namely the elastic strain component (first term on the right-hand side of Eq. (3)) and the chemical strain component (second term on the right-hand side of Eq. (3)).

The constitutive (Eq. (3)) and congruence (Eq. (4)) equations are replaced in the equilibrium equation (Eq. (5)), which is written as a function of the displacement u. The displacement u is got by integrating twice the resulting equation and applying the boundary conditions reported in Eq. (6). Radial and hoop strains are computed by replacing the displacement solution u in the congruence equation (Eq. (4)), then radial and hoop stress are computed using the constitutive equation (Eq. (3)).
The solution for displacement, stress, and strain are reported in Eqs. (8)–(10), and they can be computed once the lithium concentration is got solving the diffusive problem (Eq. (7)).

The mass transfer equation (Eq. (1)) can be rewritten to take into account the coupling between mechanical and chemical fields, as shown in previous authors' works [12]. In this case, DIS affects lithium transport through the gradient of hydrostatic stress,

according to Eq. (12).

$$\frac{\partial c}{\partial t} = \frac{D}{r^2}\frac{\partial}{\partial r}\left(r^2\frac{\partial c}{\partial r} - r^2\frac{\Omega(c-c_R)}{R_g T}\frac{\partial \sigma_h}{\partial r}\right) \tag{12}$$

where D is the diffusion coefficient, $\sigma_h = \frac{\sigma_r + 2\sigma_c}{3}$ is the hydrostatic stress, and R_g is the gas constant.
Eq. (12) can be written in the same form as the mass transfer equation reported in Eq. (1) to keep the analogy with the heat transfer equation and to use the solution reported in Eqs. (7)–(10). In this case, an equivalent concentration-dependent diffusion coefficient ($D_{eqv}(c)$) replaces the physical diffusion coefficient D in Eq. (1), as reported in Eq. (13) [12].

$$D_{eqv}(c) = D\left[1 + k_m(c - c_R)\right] \tag{13}$$

where $k_m = \frac{2\Omega^2 E}{9R_g T(1-\nu)}$ is the coefficient coupling the mechanical and chemical fields, E is the Young modulus, and ν is the Poisson ratio.

2.2. Linear elastic fracture mechanics theory

According to the LEFM theory, the stress at the crack tip is infinite, thus suitable parameters are needed to properly describe the stress field near the crack tip.
The SIF (K) is a well-established parameter used to quantify the singularity of the stress field near the crack tip, according to Eq. (14) [3].

$$\sigma_{ij} = \frac{K}{\sqrt{2\pi r_c}} f_{ij}(\theta) \tag{14}$$

Where σ_{ij} are the components of the stress tensor, r_c and θ are the polar coordinates with the origin at the crack tip and $f_{ij}(\theta)$ is a dimensionless shape function.

SIF is generally computed analytically in the case of simple geometry and loading condition, on the other hand, numerical computation based on FEM is often used for cases involving arbitrary cracks in complex structures or under complex loading conditions.

2.2.1. Stress intensity factor — numerical computation

The SIF is generally computed with FEM using the J-integral, which is a contour integral developed by Rice [62] to characterize the crack tip state both in linear elastic and elastic–plastic materials.

The standard form of J-integral proposed by Rice [62] for 2D fracture problem is reported in Eq. (15), considering an arbitrary counterclockwise path Γ around the crack tip (Fig. 1).

$$J = \int_\Gamma \left(W\,dx_2 - \mathbf{t}\cdot\frac{\partial \mathbf{u}}{\partial x_1}\,ds\right) \tag{15}$$

where $W = \int_0^{\epsilon_{ij}} \sigma_{ij}\,d\epsilon_{ij}$ (Einstein notation) is the strain energy density, σ_{ij} and ε_{ij} are the components of the stress and strain tensors, $\mathbf{u}$ is the displacement vector, $\mathbf{t}$ is the traction vector acting on the path Γ and its components are $t_i = \sigma_{ij}n_j$, n_j is the versor normal to Γ, x_1 and x_2 are the coordinate directions, and ds is the element length along the path Γ.

Rice demonstrated that the J-integral is path-independent, meaning that its value does not depend on the chosen path Γ.
However, the standard form of J-integral is no longer path-independent in thermo-mechanical [63,64] or mechanical-diffusive [33–35] fracture problems. In this case, the modified expression of J-integral (J^{DF}) keeping the path-independence property is

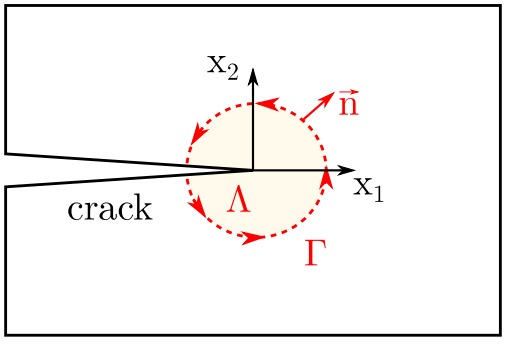

Fig. 1. Scheme of the crack region, where Γ is an arbitrary counterclockwise path surrounding the crack tip, Λ is the area enclosed by the path Γ, x_1, x_2 are the coordinate directions and $\vec{n}$ is the versor normal to Γ.

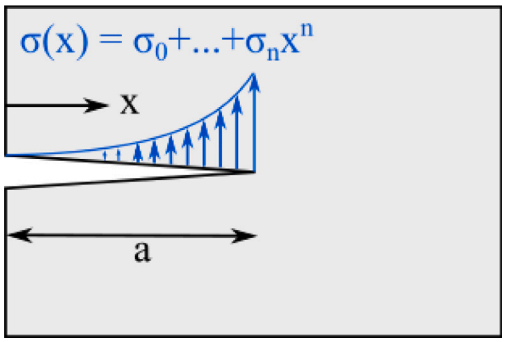

Fig. 2. Polynomial stress distribution applied on the crack surface, where x is the coordinate along the crack surface and a is the crack length.

reported in Eq. (16).

$$J^{DF} = \int_{\Gamma}\left(W\,dx_2 - \mathbf{t}\cdot\frac{\partial \mathbf{u}}{\partial x_1}\,ds\right) + \int_{\Lambda}\left(\boldsymbol{\sigma}^{P}\cdot\frac{\partial \boldsymbol{\epsilon}^{DF}}{\partial x_1}\,d\Lambda\right) \tag{16}$$

Where Λ is the area enclosed within the path Γ, $\boldsymbol{\sigma}^{P} = [\sigma_{11}, \sigma_{22}, \sigma_{33}]$ is the vector of the principal stresses, $\boldsymbol{\epsilon}^{DF}$ is the strain vector due to the diffusive fields, i.e. the chemical (Eq. (11)a) or thermal field (Eq. (11)b).
Eq. (16) states that the energy related to thermal or chemical strain (the second term on the right-hand side of Eq. (16)) has to be added to the standard J-integral expression developed by Rice (the first term on the right-hand side of Eq. (16)) in order to satisfy the energy balance and to ensure the path-independence property of J-integral.

The J-integral is equal to the energy release rate G when the LEFM theory holds, then SIF can be computed from the J-integral according to Eq. (17).

$$K = \begin{cases} \sqrt{JE} & \text{plane stress} \\ \sqrt{\frac{JE}{(1-\nu^2)}} & \text{plane strain} \end{cases} \tag{17}$$

2.2.2. Stress intensity factor — analytical computation

The SIF K can be analytically computed using the dimensionless geometric factor Y according to Eq. (18) [3].

$$K = Y\sigma\sqrt{a} \tag{18}$$

Where a is the crack size and σ is the nominal stress in the far-field, i.e. the stress unaffected by the geometrical discontinuity of the crack. The geometric factor Y accounts for the specimen geometry, as well as the size, location, and shape of the crack. Once the geometric factor is known, the SIF can be computed for any combination of σ and a, as long as the loading conditions are the same.
A large number of geometric factors for various crack geometries are published in the literature and tabulated in several handbooks [7,8,65]. These geometric factors are obtained considering simple loading cases, namely tension, bending, or their combination, resulting in a constant or linear stress distribution on the crack surfaces. Then, a more complex loading condition requires the determination of new geometric factor.

Alternatively, the principle of superposition of effects is used in this work to compute the SIF resulting from an arbitrary stress distribution on the crack surfaces, thanks to the hypothesis of linear elasticity.
First, the arbitrary stress distribution in the uncracked body over the region where the crack is located is expressed by a polynomial of grade n, according to Eq. (19).

$$\sigma(x) = \sum_{i=0}^{n}\sigma_i x^i \tag{19}$$

Where σ_i are the coefficients of the polynomial and x is the coordinate along the crack surface and it is positive moving toward the crack tip (Fig. 2).

Then, the SIF (K) is computed by combining Eqs. (19) and (18) and using the principle of superposition of effects, according to Eq. (20).

$$K = \sum_{i=0}^{n} Y_i\sigma_i x^i\sqrt{a} \tag{20}$$

Where Y_i is the geometric factor for the specific crack configuration corresponding to the ith term of the polynomial stress distribution.

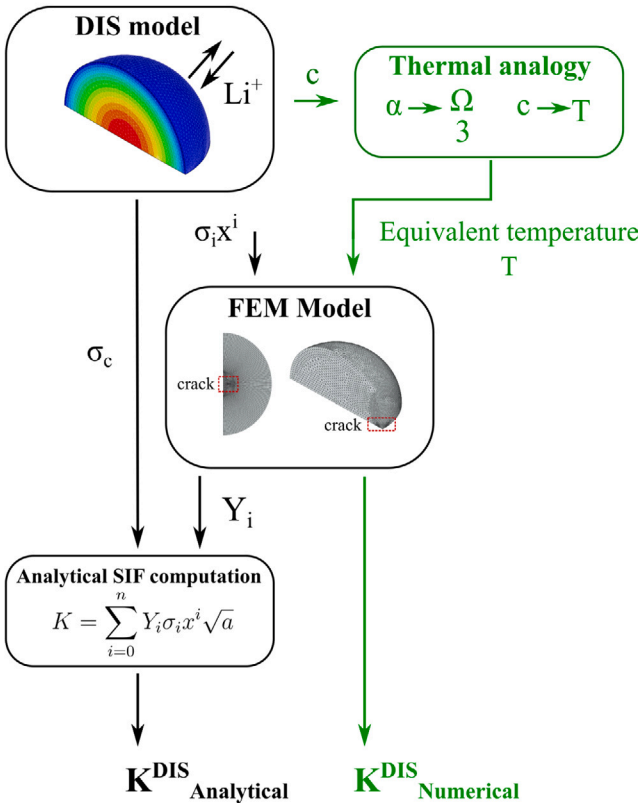

Fig. 3. Analytical procedure for SIF computation, where the validation procedure is reported in green.

2.3. Procedure for analytical SIF computation

The analytical procedure developed for SIF computation in case of arbitrary stress distribution on crack surfaces is deepened in this section. According to Fig. 3, a FEM model is implemented to compute geometric factors. Then, these geometric factors are used to analytically compute the SIF based on the stress distribution resulting from DIS model. Finally, the analytical computation is validated with the SIF numerically computed using the FEM model.

2.3.1. FEM model

A FEM model is built in Ansys Mechanical APDL aiming: (a) to compute the geometric factors for a sphere with central and superficial cracks. These geometric factors are generic and can be used for any arbitrary polynomial stress distribution; (b) to compute SIF due to DIS in active material particles of LIBs electrodes and to validate the results of the analytical computation of SIF based on the geometric factors obtained according to point a.

Fig. 4 shows the geometry of the sphere with central and superficial cracks. The central crack has the shape of a disk with diameter of $2a$ (Fig. 4a), on the other hand, the superficial crack is a semi-circle with crack depth of a (Fig. 4e). The sphere with the central crack is modeled in 2D exploiting the axisymmetry. On the other hand, a 3D model is built for the sphere with superficial crack, and just half of the sphere is modeled thanks to the symmetry.

The mesh is composed of PLANE183 elements in axisymmetric mode for the 2D model (Fig. 4b–d) and SOLID186 elements for the 3D model (Fig. 4f–h). Special care is taken for the mesh near the crack region. Singular elements are used to capture the $\frac{1}{\sqrt{r_c}}$ singularity of the stress field [66], then the elements are chosen to be small near the crack region, and their size is gradually increased when moving away from it.

The reader can refer to previous authors' works for a detailed description of the strategy to build the FEM model and mesh [25,37].

2.3.2. Geometric factors computation

The geometric factors for sphere with central and superficial cracks depend just on the ratio a/R. Each geometric factor (Y_i) corresponding to the single grade of the polynomial stress distribution is determined as summarized below, chosen the ratio a/R.

1. The single grade of the polynomial stress distribution ($\sigma_i x^i$) is applied as a pressure load on nodes of the crack line (2D model) and the crack surface (3D model).

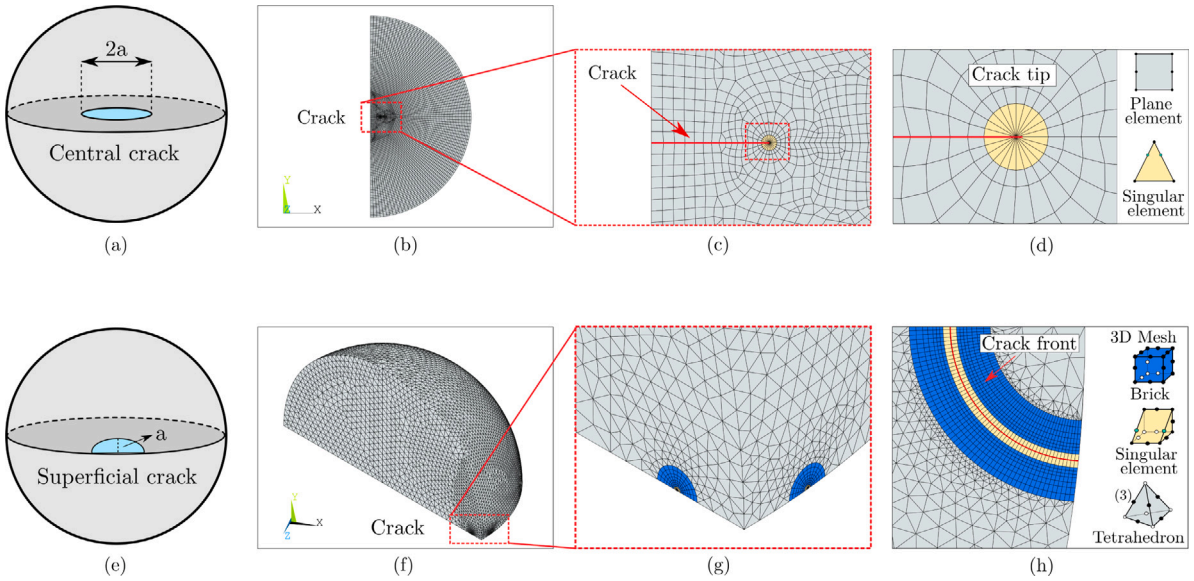

Fig. 4. (a) Geometry of sphere with disk-shaped crack located at the center, (b) corresponding 2D axisymmetric FEM mesh model with detail of (c) crack tip region and (d) elements around crack tip region. (e) Geometry of sphere with semi-circular crack located on the surface, (f) corresponding 3D FEM mesh model with detail of (g) crack region and (h) elements around the crack region (bottom view).

2. The corresponding SIF (K_i^{FEM}) is computed from the J-integral using the CINT command in Ansys, according to Eq. (17).
3. The geometric factor Y_i is estimated using Eq. (20), as reported in Eq. (21).

$$Y_i = \frac{K_i^{FEM}}{\sigma_i a^i \sqrt{a}} \qquad i \in \{0, 1, \dots, n\} \tag{21}$$

The procedure is repeated considering another value of a/R, then closed-form expressions of the geometric factors are computed as a function of a/R.

2.3.3. SIF computation in case of DIS

DIS model presented in Section 2.1 is used to compute the hoop stress distribution in the uncracked particle over the region where the crack is located. Then, the hoop stress is approximated with a polynomial and the SIF is analytically computed according to Eq. (20), using the geometric factors computed as reported in Section 2.3.2.

SIF is also computed numerically with FEM in order to validate the analytical results. In this case, the concentration distribution within the active material particle is computed analytically according to DIS model reported in Section 2.1. Then, the concentration is converted into the equivalent temperature exploiting the analogy between diffusive and thermal equations [25,37]. The equivalent temperature is mapped on structural nodes of the FEM model including the crack surfaces. Finally, SIF is computed from the J-integral using the CINT command in Ansys, according to Eq. (17).

3. Results and discussion

The geometric factors computed for sphere with central and superficial cracks are reported in this section. Then, SIF due to the hoop stress resulting from lithium diffusion in active material particles is analytically computed, according to Section 2.3.3. Finally, the analytical results are compared with FEM fracture model results.

3.1. Geometric factors results

In this work, the geometric factors are computed considering a polynomial of grade 6, then, seven geometric factors are computed according to the procedure previously reported in Section 2.3.2. In other applications, if the stress distribution can be satisfactorily fitted with a polynomial of lower grade, geometric factors of higher order can be neglected accordingly.
Figs. 5 and 6 show the geometric factors for the sphere with central and superficial cracks, respectively.

The results show that the geometric factors are quadratic functions of the normalized crack length a/R. Tables 2 and 3 provide closed-form expressions for these geometric factors.

The values of geometric factor corresponding to a constant stress distribution on the surfaces of central crack (Y_0) are in agreement with the values reported in the literature by Reinhardt et al. in [67].

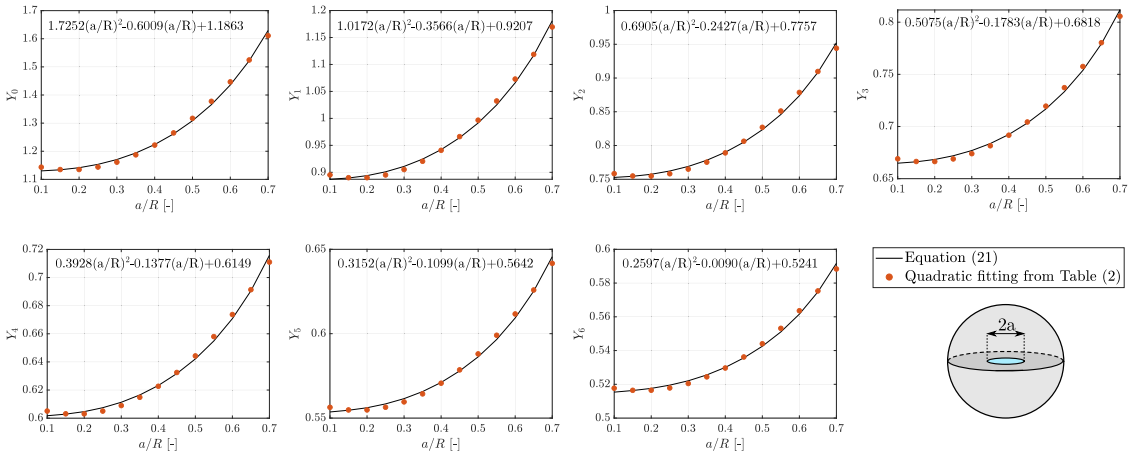

Fig. 5. Geometric factors Y_i for sphere with central crack. The curves in black refer to values obtained combining FEM solutions and Eq. (21), on the other hand, the red dots result from the fitting with quadratic functions $(p(\frac{a}{R})^2 + q(\frac{a}{R}) + r)$.

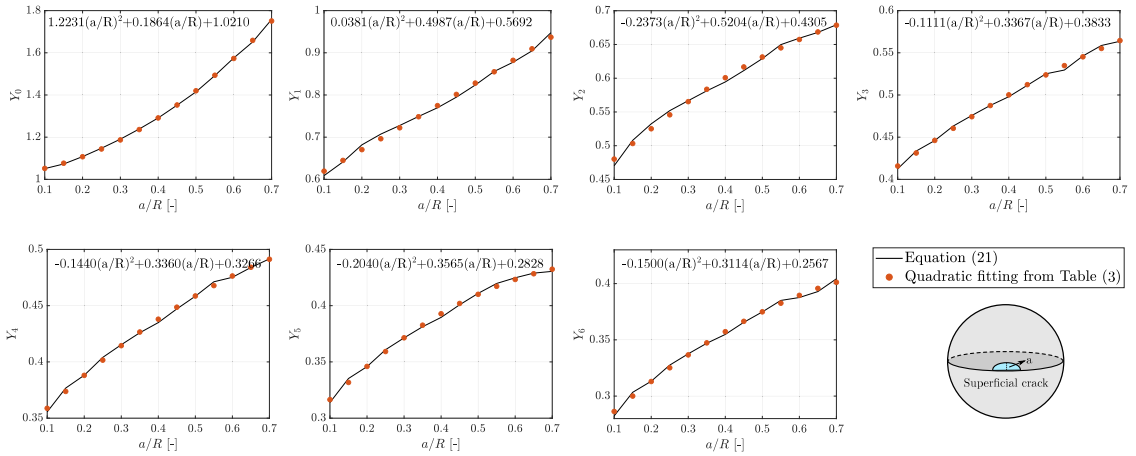

Fig. 6. Geometric factors Y_i for sphere with superficial crack. The curves in black refer to values obtained combining FEM solutions and Eq. (21), on the other hand, the red dots result from the fitting with quadratic functions $(p(\frac{a}{R})^2 + q(\frac{a}{R}) + r)$.

Table 2
Coefficients of the quadratic function $p(\frac{a}{R})^2 + q(\frac{a}{R}) + r$ for geometric factors of sphere with central crack.

Geometric factor	p	q	r
Y_0	1.7252	−0.6009	1.1863
Y_1	1.0172	−0.3566	0.9207
Y_2	0.6905	−0.2427	0.7757
Y_3	0.5075	−0.1783	0.6818
Y_4	0.3928	−0.1377	0.6149
Y_5	0.3152	−0.1099	0.5642
Y_6	0.2597	−0.0900	0.5241

Table 3
Coefficients of the quadratic function $p(\frac{a}{R})^2 + q(\frac{a}{R}) + r$ for geometric factors of sphere with superficial crack.

Geometric factor	p	q	r
Y_0	1.2231	0.1864	1.0210
Y_1	0.0381	0.4987	0.5692
Y_2	−0.2373	0.5204	0.4305
Y_3	−0.1111	0.3367	0.3833
Y_4	−0.1440	0.3360	0.3266
Y_5	−0.2040	0.3565	0.2828
Y_6	−0.1500	0.3114	0.2567

Table 4
Graphite properties [12].

Property	Symbol	Value	Unit
Radius	R	10×10^{-6}	m
Young modulus	E	15	MPa
Poisson ratio	ν	0.3	–
Partial molar volume	Ω	4.2×10^{-6}	m^3/mol
Diffusion coefficient	D	2×10^{-14}	m^2/s
Maximum concentration	c_{max}	2.9155×10^4	mol/m^3
Temperature	T	298	K

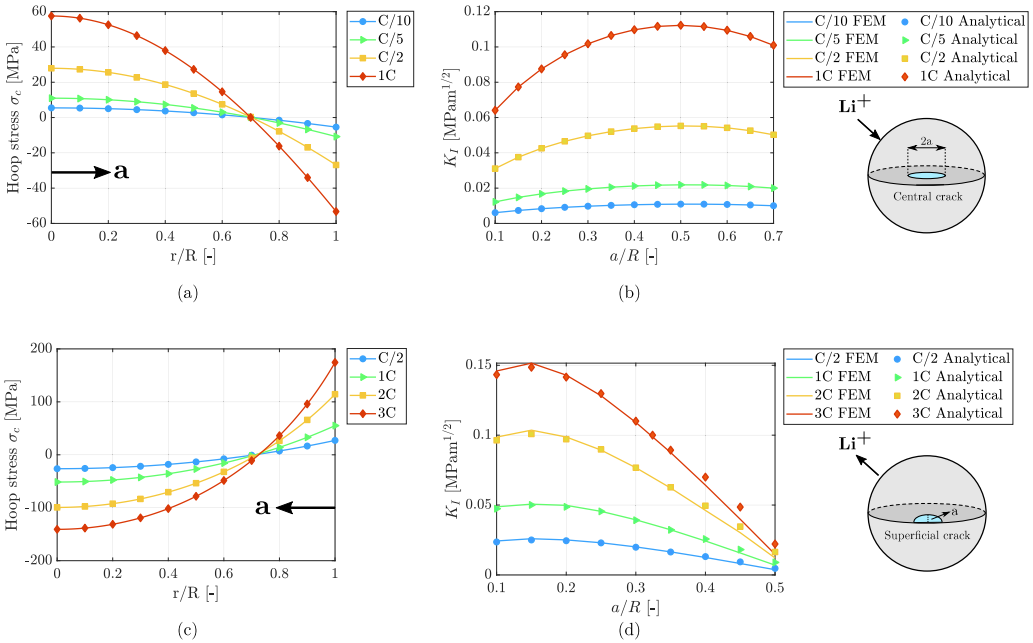

Fig. 7. Results of DIS and fracture model for graphite particle varying C-rate at 50% SOC. Hoop stress distribution (a) during lithium insertion and (c) during lithium extraction. SIF values varying a/R for (b) particle with central crack during lithium insertion and (d) particle with superficial crack during lithium extraction.

3.2. Numerical validation of the analytical method in case of DIS

SIF due to the hoop stress caused by lithium diffusion in active material particles of LIB electrodes is computed both analytically using the geometric factors reported in Tables 2 and 3 and numerically with the FEM fracture model described in Section 2.3.1. The results are provided in this section.

The electrochemical–mechanical problem is solved analytically according to DIS model reported in Section 2.1, including the coupling between chemical and mechanical fields. A constant flux is applied at the particle boundary using Eq. (2), according to the current delivered by the battery.

On the following, the C-rate equal to 1 allows completely filling (or emptying) the active material particle in one hour. Furthermore, the SOC is intended as the percentage of lithium ions within the particle relative to the maximum concentration ($SOC = \frac{c}{c_{max}}$).

A graphite particle is chosen as a case study and the corresponding physical parameters are reported in Table 4.

Lithium insertion is considered for the particle with central crack, on the other hand, lithium extraction is considered for particle with superficial crack, as they trigger tensile hoop stress on the particle center and surface, respectively.

Fig. 7a,c shows the hoop stress distribution within the graphite particle during lithium insertion and extraction respectively, varying the C-rate and considering 50% SOC. The results show that higher C-rate causes higher concentration gradients within active material particles, then higher stress, as also reported in previous authors' works [12].

SIF values computed analytically with the geometric factors reported in Tables 2 and 3 are compared to the results derived numerically with the FEM model in Fig. 7b,d, varying the crack length and C-rate. The comparison shows a perfect agreement, demonstrating the validity of the analytical procedure proposed in this work for SIF computation in the case of non-constant stress distribution on crack surfaces.

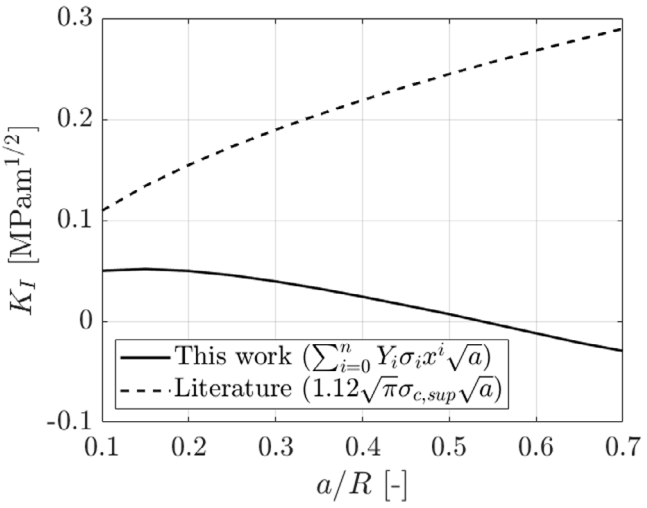

Fig. 8. Comparison between SIF values computed with the analytical procedure developed in this work and the approximation of plates and constant stress distribution usually made in the literature ($K = 1.12\sqrt{\pi}\sigma_{c,sup}\sqrt{a}$, where $\sigma_{c,sup}$ is the hoop stress on the particle surface). Graphite particle with superficial crack during lithium extraction at 1C and 50% SOC is considered. The dotted line shows where the SIF changes sign.

Furthermore, the results show that both C-rate, then the hoop stress within the particle, and crack length affect SIF, according to Eq. (20). Higher C-rate is more detrimental from the fracture point of view because results in higher SIF, as also reported in previous authors' works [25] and confirmed by experimental measurements [68,69].
On the other hand, longer crack results in higher SIF as long as the normalized crack length is lower than $a/R = 0.5$ for particle with central crack and $a/R = 0.15$ for particle with superficial crack. Beyond these limits, the increase in crack length leads to a decrease in SIF, because of the non-constant far field stress driving the crack.
SIF variation with the crack length is attributed to the variation of the hoop stress distribution according to the radial coordinate. Indeed, the hoop stress decreases and becomes compressive going from the particle core to the surface for lithium insertion (Fig. 7a) and going from the particle surface to the core for lithium extraction (Fig. 7c). Then, longer crack experiences lower hoop stress than smaller crack because the crack tip gets closer to the compressive (or less tension) region. Then, referring to Eq. (20), an increase in the crack length increases the SIF as long as it balances the decrease in the hoop stress.

Multiphysics FEM fracture model simulations require significant computational capacity and long simulation times, which can vary from minutes to some hours or even more in the cases of simulation of fracture due to LIB cycling. On the contrary, the computational time is reduced to a few seconds when using the proposed analytical procedure, because just a sum of products is required to compute SIF. Simulation time should be kept as low as possible with the perspective of developing an aging model to assess the capacity fade due to LIB cycling as well as to estimate in real-time the remaining useful life of LIB. Then, the proposed analytical computation of SIF represents the best compromise to simulate the effect of fracture on battery degradation in terms of accuracy and computational cost.

Several works in the literature deal with fracture in active material particles due to repeated charge/discharge cycles. In this case, Paris' law is often applied to quantify the increase of crack length with cycling. However, SIF is generally computed neglecting the non-constant stress distribution on crack surfaces, directly using Eq. (18), where the far-field stress is the hoop stress on the surface of the uncracked particle. Furthermore, the geometric factor of plate under uniaxial stress ($Y_0 = 1.12\sqrt{\pi}$ [1]) is used instead of the one corresponding to spherical geometry [70–74].
A comparison between SIF values computed using the analytical procedure proposed in this work and the approximation of plate and constant stress distribution usually made in the literature is shown in Fig. 8. Particle with superficial crack during lithium extraction at 1C and 50% SOC is considered.

The results show that the difference between SIF values is small as long as a/R is lower than 0.15, on the other hand, the difference increases as a/R increases. Indeed, the decrease of SIF with the increase of crack length is not captured when using the superficial hoop stress instead of considering the entire stress distribution on crack surfaces. Furthermore, the geometric factor of plate is far from the case of spherical geometry. Then, this approximation affects the accuracy of Paris' law in assessing the increase of crack length, and consequently the results of the degradation model estimating the capacity loss of LIB with cycling.

In this work, the effect of the geometric discontinuity of the crack on lithium concentration is not modeled as SIF is computed using the hoop stress distribution of uncracked particle. However, lithium accumulates at the crack tip due to the coupling between chemical and mechanical fields, as reported in previous authors' work [25]. This causes the material near the crack tip to expand, decreasing the elastic component of deformation, and stress in turn. However, the difference between SIF values computed with the analytical procedure presented in this work and using the multiphysics FEM model considering the full coupling between fracture, chemical, and mechanical fields is less than 3%. Then, this difference can be considered acceptable, especially from the perspective of avoiding expensive multiphysics FEM simulations and limiting the computational effort of SIF computation.

4. Conclusions

This work presents a general analytical procedure to compute the SIF resulting from arbitrary stress distribution on the crack surfaces. In particular, this method can be applied in case of diffusion induced stress, caused by the diffusion of chemical species and thermal diffusion. In this case, the well-established analytical expression of SIF, i.e. the geometric factor Y multiplied by the remote stress σ and square root of crack length a ($K = Y\sigma\sqrt{a}$), cannot be applied as the stress on crack surfaces is non-constant.

Firstly, the generic stress distribution on crack surfaces is approximated by a polynomial function. Then, the SIF is computed according to the principle of superposition of effects, as the sum of the products between each individual polynomial grade and the corresponding geometric factor.

The geometric factors for sphere with central and superficial cracks are computed with a FEM fracture model built in Ansys Mechanical APDL and are expressed as a function of the normalized crack length a/R. These geometric factors are general and can be used for any kind of stress distribution.

Diffusion induced stresses are of particular interest in LIB because they are one of the most significant causes of degradation. For this reason, the developed analytical procedure is applied to compute the SIF in active material particles of LIBs electrode, where the diffusion of lithium ions causes an inhomogeneous concentration, leading to nonlinear stress distribution on crack surfaces, which drives crack propagation. SIF values resulting from the analytical computation are compared with the multiphysics FEM fracture model results, showing good agreement.

The proposed analytical computation is more accurate than the traditional analytical approach used in the literature, which instead relies on the geometric factor of plates and neglects the non-constant stress distribution on crack surfaces. Furthermore, the proposed analytical computation of SIF requires just the stress distribution resulting from the concentration gradient in particles without cracks, which can be obtained using well-established closed-form solutions. Then, SIF is computed by performing a sum of products, running in a few seconds and being faster and less computationally demanding compared to solving multiphysics FEM fracture models, whose simulation time ranges between minutes to some hours. Then, the proposed analytical procedure can be used to assess fracture in active material particles due to charge/discharge cycles, with the perspective of developing fast, accurate, and computationally efficient degradation models for the online estimation of LIBs capacity decay.

CRediT authorship contribution statement

Francesca Pistorio: Writing – original draft, Validation, Software, Methodology, Conceptualization. **Davide Clerici:** Writing – review & editing, Conceptualization. **Aurelio Somà:** Writing – review & editing, Supervision, Project administration, Conceptualization.

Declaration of competing interest

The authors declare that they have no known competing financial interests or personal relationships that could have appeared to influence the work reported in this paper.

Data availability

No data was used for the research described in the article

References

[1] Anderson TL. Fracture mechanics: Fumdamental and applications. 2017, p. 668.
[2] Broek D. Elementary engineering fracture mechanics. Springer Science & Business Media; 2012.
[3] Irwin GR. Analysis of stresses and strains near the end of a crack traversing a plate. J Appl Mech 2021;24(3):361–4.
[4] Erdogan F, Sih GC. On the crack extension in plates under plane loading and transverse shear. J Basic Eng 1963;85:519–25.
[5] Paris P, Erdogan F. A critical analysis of crack propagation laws. J Basic Eng 1963;85(4):528–33.
[6] Pistorio F, Soma' A. Fatigue fracture mechanics in gold-based MEMS notched specimens: experimental and numerical study. J Micromech Microeng 2023.
[7] Murakami Y, Keer LM. Stress intensity factors handbook, vol. 3. J Appl Mech 1993;60(4):1063.
[8] Tada H, Paris PC, Irwin GR. The stress analysis of cracks handbook. 3rd ed.. ASME Press; 2000.
[9] Sih GC. Handbook of stress-intensity factors: Stress-intensity factor solutions and formulas for reference. Bethlehem, Pa.: Lehigh University; 1973, p. 815, 1973.
[10] Al Laham S, Branch SI. Stress intensity factor and limit load handbook, Vol. 3. British Energy Generation Limited Gloucester, UK; 1998.
[11] Prussin S. Generation and distribution of dislocations by solute diffusion. J Appl Phys 1961;32(10):1876–81.
[12] Clerici D, Mocera F, Somà A. Analytical solution for coupled diffusion induced stress model for lithium-ion battery. Energies 2020;13(7):1717.
[13] Hellen T, Cesari F, Maitan A. The application of fracture mechanics in thermally stressed structures. Int J Press Vessels Pip 1982;10(3):181–204.
[14] Matsuda S, Takenaka J, Arii K, Ogi K. Cyclic fatigue life characteristics of ceramic balls under variable thermal shock loadings. Eng Fract Mech 2021;255:107924.
[15] Matsuda S. Fracture characteristics of silicon nitride ceramic ball subjected to thermal shock. J Mater Sci 2016;51:5502–13.
[16] Strobl S, Adlmann F-A, Supancic P, Lube T, Danzer R, Schöppl O. Fracture toughness of silicon nitride balls via thermal shock. J Eur Ceram Soc 2018;38(4):1278–87.
[17] Oliveira R, Wu X. Stress intensity factors for axial cracks in hollow cylinders subjected to thermal shock. Eng Fract Mech 1987;27(2):185–97.
[18] Lee KY, Kwan-Bo S. Thermal shock stress intensity factor by Bueckner's weight function method. Eng Fract Mech 1990;37(4):799–804.

[19] Emmel E, Stamm H. Calculation of stress intensity factors of thermally loaded cracks using the finite element method. Int J Press Vessels Pip 1985;19(1):1–17.
[20] Thamaraiselvi K, Vishnuvardhan S. Fracture studies on reactor pressure vessel subjected to pressurised thermal shock: A review. Nucl Eng Des 2020;360:110471.
[21] Li P, Zhao Y, Shen Y, Bo S-H. Fracture behavior in battery materials. J Phys: Energy 2020;2(2):022002.
[22] Mocera F, Somà A, Clerici D. Study of aging mechanisms in lithium-ion batteries for working vehicle applications. In: 2020 fifteenth international conference on ecological vehicles and renewable energies (EVER). IEEE; 2020, p. 1–8.
[23] Pistorio F, Clerici D, Mocera F, Somà A. Review on the experimental characterization of fracture in active material for Lithium-Ion batteries. Energies 2022;15(23):9168.
[24] Pistorio F, Clerici D, Mocera F, Somà A. Review on the numerical modeling of fracture in active materials for lithium ion batteries. J Power Sources 2023;566:232875.
[25] Pistorio F, Clerici D, Mocera F, Somà A. Coupled electrochemical–mechanical model for fracture analysis in active materials of lithium ion batteries. J Power Sources 2023;580:233378.
[26] Deshpande R, Cheng Y-T, Verbrugge MW. Modeling diffusion-induced stress in nanowire electrode structures. J Power Sources 2010;195(15):5081–8.
[27] Zhao Y, Stein P, Bai Y, Al-Siraj M, Yang Y, Xu B-X. A review on modeling of electro-chemo-mechanics in lithium-ion batteries. J Power Sources 2019;413:259–83.
[28] Clerici D, Mocera F, Somà A. Analytical solution for coupled diffusion induced stress model for Lithium-Ion battery. Energies 2020;13(7).
[29] Clerici D, Mocera F, Somà A. Shape influence of active material micro-structure on diffusion and contact stress in Lithium-Ion batteries. Energies 2021;14(1).
[30] Clerici D, Mocera F. Micro-scale modeling of lithium-ion battery. IOP Conf Ser: Mater Sci Eng 2021;1038(1):012007.
[31] Clerici D, Mocera F, Somà A. Experimental characterization of Lithium-Ion cell strain using laser sensors. Energies 2021;14(19).
[32] Clerici D, Mocera F, Somà A. Electrochemical–mechanical multi-scale model and validation with thickness change measurements in prismatic lithium-ion batteries. J Power Sources 2022;542:231735.
[33] Gao YF, Zhou M. Coupled mechano-diffusional driving forces for fracture in electrode materials. J Power Sources 2013;230:176–93.
[34] Haftbaradaran H, Qu J. A path-independent integral for fracture of solids under combined electrochemical and mechanical loadings. J Mech Phys Solids 2014;71(1):1–14.
[35] Zhang M, Qu J, Rice JR. Path independent integrals in equilibrium electro-chemo-elasticity. J Mech Phys Solids 2017;107:525–41.
[36] Cai X, Guo Z. Coupled mechano-diffusion J-integral in active particles under the influence of binder. Eng Fract Mech 2020;231:107031.
[37] Clerici D, Mocera F, Pistorio F. Analysis of fracture behaviour in active materials for lithium ion batteries. In: IOP conference series: materials science and engineering, Vol. 1214. IOP Publishing; 2022, 012018.
[38] Woodford WH, Chiang Y-M, Carter WC. Electrochemical shock" of intercalation electrodes: a fracture mechanics analysis. J Electrochem Soc 2010;157(10):A1052.
[39] Raghavan RS, Kumar AM, Narayanrao R. Intercalation induced surface cracking in electrode particles. ZAMM-J Appl Math Mech/Z Angew Math Mech 2015;95(8):845–58.
[40] Singh A, Pal S. Coupled chemo-mechanical modeling of fracture in polycrystalline cathode for lithium-ion battery. Int J Plast 2020;127:102636.
[41] Chen B, Zhou J, Cai R. Analytical model for crack propagation in spherical nano electrodes of lithium-ion batteries. Electrochim Acta 2016;210:7–14.
[42] Sarkar A, Shrotriya P, Chandra A. Fracture modeling of lithium-silicon battery based on variable elastic moduli. J Electrochem Soc 2017;164(11):E3606.
[43] Ryu I, Choi JW, Cui Y, Nix WD. Size-dependent fracture of Si nanowire battery anodes. J Mech Phys Solids 2011;59(9):1717–30.
[44] Grantab R, Shenoy VB. Location-and orientation-dependent progressive crack propagation in cylindrical graphite electrode particles. J Electrochem Soc 2011;158(8):A948.
[45] Sun G, Sui T, Song B, Zheng H, Lu L, Korsunsky AM. On the fragmentation of active material secondary particles in lithium ion battery cathodes induced by charge cycling. Extreme Mech Lett 2016;9:449–58.
[46] Xu R, Zhao K. Corrosive fracture of electrodes in Li-ion batteries. J Mech Phys Solids 2018;121:258–80.
[47] Zhang Y, Guo Z. Numerical computation of central crack growth in an active particle of electrodes influenced by multiple factors. Acta Mech Sinica 2018;34:706–15.
[48] Zhang Y, Zhao C, Guo Z. Simulation of crack behavior of secondary particles in Li-ion battery electrodes during lithiation/de-lithiation cycles. Int J Mech Sci 2019;155:178–86.
[49] Bai Y, Zhao K, Liu Y, Stein P, Xu B-X. A chemo-mechanical grain boundary model and its application to understand the damage of Li-ion battery materials. Scr Mater 2020;183:45–9.
[50] Tian H, Gao L, Huang P, Li Y, Guo Z-S. Simulation of intergranular fracture behavior inside randomly aggregated LiNixCoyMn1-x-yO2 polycrystalline particle. Eng Fract Mech 2022;266:108381.
[51] Miehe C, Dal H, Schänzel L-M, Raina A. A phase-field model for chemo-mechanical induced fracture in lithium-ion battery electrode particles. Internat J Numer Methods Engrg 2016;106(9):683–711.
[52] Ahmadi M. A hybrid phase field model for fracture induced by lithium diffusion in electrode particles of Li-ion batteries. Comput Mater Sci 2020;184:109879.
[53] Singh A, Pal S. Chemo-mechanical modeling of inter-and intra-granular fracture in heterogeneous cathode with polycrystalline particles for lithium-ion battery. J Mech Phys Solids 2022;163:104839.
[54] Xue R, Li X, Zhao H, Chen Z. Phase field model coupling with strain gradient plasticity for fracture in lithium-ion battery electrodes. Eng Fract Mech 2022;269:108518.
[55] Ai W, Wu B, Martínez-Pañeda E. A coupled phase field formulation for modelling fatigue cracking in lithium-ion battery electrode particles. J Power Sources 2022;544:231805.
[56] Klinsmann M, Rosato D, Kamlah M, McMeeking RM. Modeling crack growth during Li insertion in storage particles using a fracture phase field approach. J Mech Phys Solids 2016;92:313–44.
[57] Mesgarnejad A, Karma A. Phase field modeling of chemomechanical fracture of intercalation electrodes: Role of charging rate and dimensionality. J Mech Phys Solids 2019;132:103696.
[58] Boyce AM, Martínez-Pañeda E, Wade A, Zhang YS, Bailey JJ, Heenan TM, Brett DJ, Shearing PR. Cracking predictions of lithium-ion battery electrodes by X-ray computed tomography and modelling. J Power Sources 2022;526:231119.
[59] T O'Connor D, Welland MJ, Liu WK, Voorhees PW. Phase transformation and fracture in single LixFePO4 cathode particles: a phase-field approach to Li–ion intercalation and fracture. Modelling Simul Mater Sci Eng 2016;24(3):035020.
[60] Liu B, Xu J. Cracks of silicon nanoparticles in anodes: Mechanics–electrochemical-coupled modeling framework based on the phase-field method. ACS Appl Energy Mater 2020;3(11):10931–9.
[61] Xu B-X, Zhao Y, Stein P. Phase field modeling of electrochemically induced fracture in Li-ion battery with large deformation and phase segregation. GAMM-Mitt 2016;39(1):92–109.
[62] Rice JR. A path independent integral and the approximate analysis of strain concentration by notches and cracks. J Appl Mech 1968;35(2):379–86.
[63] Aoki S, Kishimoto K, Sakata M. Elastic-plastic analysis of crack in thermally-loaded structures. Eng Fract Mech 1982;16(3):405–13.
[64] Kishimoto K, Aoki S, Sakata M. On the path independent integral- J. Eng Fract Mech 1980;13(4):841–50.

[65] Rooke DP, Cartwright DJ. Compendium of stress intensity factors. Procurement Executive, Ministry of Defence. H. M. S. O.; 1976, p. 330, 1976, (Book).
[66] Barsoum RS. On the use of isoparametric finite elements in linear fracture mechanics. Internat J Numer Methods Engrg 1976;10(1):25–37.
[67] Reinhardt H, Mielich O. A fracture mechanics approach to the crack formation in alkali-sensitive grains. Cem Concr Res 2011;41(3):255–62.
[68] Chen D, Kramer D, Mönig R. Chemomechanical fatigue of limn1. 95Al0. 05o4 electrodes for lithium-ion batteries. Electrochim Acta 2018;259:939–48.
[69] Lin N, Jia Z, Wang Z, Zhao H, Ai G, Song X, Bai Y, Battaglia V, Sun C, Qiao J, et al. Understanding the crack formation of graphite particles in cycled commercial lithium-ion batteries by focused ion beam-scanning electron microscopy. J Power Sources 2017;365:235–9.
[70] Deshpande R, Verbrugge M, Cheng Y-T, Wang J, Liu P. Battery cycle life prediction with coupled chemical degradation and fatigue mechanics. J Electrochem Soc 2012;159(10):A1730.
[71] Shao J, Li J, Yuan W, Dai C, Wang Z, Zhao M, Pecht M. A novel method of discharge capacity prediction based on simplified electrochemical model-aging mechanism for lithium-ion batteries. J Energy Storage 2023;61:106788.
[72] Purewal J, Wang J, Graetz J, Soukiazian S, Tataria H, Verbrugge MW. Degradation of lithium ion batteries employing graphite negatives and nickel–cobalt–manganese oxide+ spinel manganese oxide positives: Part 2, chemical–mechanical degradation model. J Power Sources 2014;272:1154–61.
[73] Hwang G, Sitapure N, Moon J, Lee H, Hwang S, Kwon JS-I. Model predictive control of lithium-ion batteries: Development of optimal charging profile for reduced intracycle capacity fade using an enhanced single particle model (SPM) with first-principled chemical/mechanical degradation mechanisms. Chem Eng J 2022;435:134768.
[74] Zhang K, Zhou J, Tian T, Kai Y, Li Y, Zheng B, Yang F. Cycling-induced damage of silicon-based lithium-ion batteries: Modeling and experimental validation. Int J Fatigue 2023;172:107660.